CrossMark

A New Statistical Distance Scale for Planetary Nebulae, Based on Gaia EDR3

A. Ali[1] , E. Algarni[2], A. Mindil[3], and S. A Alghamdi[2]
[1] Astronomy, Space Science & Meteorology Department, Faculty of Science, Cairo University, Giza 12613, Egypt; afouad@sci.cu.edu.eg
[2] Astronomy and Space Science Department, Faculty of Science, King Abdulaziz University, Jeddah, Saudi Arabia
[3] Department of Physics, College of Science, University of Jeddah, Jeddah, Saudi Arabia; amindil@uj.edu.sa

Abstract

The present work aims to build a new statistical distance scale for planetary nebulae (PNe) based on a rigorous calibration sample. The distances of the calibration sample are derived from the trigonometric parallax method using the recent measurements of Gaia Early Data Release 3 (Gaia EDR3). The new distance scale is created by applying the well-known linear relationship between the radio surface brightness temperature and the nebular radius. The calibration sample is made up of 96 PNe of accurately computed distances with uncertainties less than 20%. Earlier ground- and space-based trigonometric parallaxes of PNe display inconsistency with those of Gaia, particularly the Hipparcos results. In addition, these measurements have appreciably lower precision than those of Gaia. When compared to the trigonometric technique, the expansion and kinematic methods exhibited more consistency than the spectroscopic, extinction, gravity, and photoionization methods. Furthermore, contrary to earlier results in the literature, the extinction and gravity methods, on average, underestimate and slightly overestimate the PN distances respectively. As a byproduct of extracting the Gaia parallaxes, we detect the radial velocity and variability for 14 and 3 PN central stars (CSs), respectively. To our knowledge, the variability of Hen 2-447 CS has been determined for the first time.

Key words: (ISM:) planetary nebulae: general – parallaxes – stars: variables: general – stars: distances

Online material: machine-readable tables

1. Introduction

Gaia is a space mission that was launched and is operated by the European Space Agency (ESA) to provide a detailed three-dimensional (3D) map of the Milky Way Galaxy. Gaia Data Release 1 (Gaia DR1) was published in September 2016, followed by the Gaia Data Release 2 (Gaia DR2) in April 2018 and Gaia Early Data Release 3 (Gaia EDR3) in December 2020. The full Gaia Data Release 3 (Gaia DR3) is scheduled in the first part of 2022. Gaia EDR3 provides the position and apparent magnitude for $\sim$1.8 billion sources, as well as the parallax (π_{Gaia}), proper motion (μ), and (B-R) color for $\sim$1.5 billion sources. In comparison to Gaia DR2, the newest release exhibits considerable enhancements in the astrometric and photometric accuracy, precision, and homogeneity (Brown et al. 2021). The precision of the parallax and proper motion are improved by 30% and a factor of two, respectively. Moreover, the estimated parallax zero-point for Gaia EDR3, -0.017 mas (Lindegren et al. 2021), was enhanced compared with Gaia DR2, -0.029 mas (Lindegren et al. 2018).

The precise distances of planetary nebulae (PNe) enable astronomers to better understand the evolution of low and intermediate-mass stars and the entire Galaxy. Knowing the distance is a key tool for studying the significant parameters of a PN and its accompanying central star (CS). However, because of the wide variety of their characteristics, obtaining accurate distances for PNe is a difficult task. The procedures usually applied to derive the distances of PNe are known as individual and statistical methods. The description, limitations, assumptions, and uncertainties of these methods were discussed in Frew et al. (2016), hereafter FBP16. Although the trigonometric technique is the only direct and trusted individual method for defining PN distances, it is confined to nearby PNe that are linked with detected CSs. Therefore, there is still a need to apply other methods to determine the distances of remote PNe and those associated with very faint or undetectable CSs.

Any statistical method depends on a relationship between two nebular parameters, one is distance-dependent and the other is distance-independent. After calibrating such a relationship using PNe of known distances, we can use it to calculate the statistical distance to any PN. Ali et al. (2015), hereafter AIA15, have developed two statistical distance scales based on a calibration sample composed of 82 PNe. This sample is larger and more dependable than those applied in prior distance scales that were known at that time. Except for a few objects with trustworthy trigonometric, spectroscopic, and cluster membership distances, the distance of each calibrator was computed as a weighted mean value derived from at least two different individual methods. This sample was applied to recalibrate the

linear mass–radius ($M-R$) and radio surface brightness temperature-radius ($Tb-R$) relationships. The main goal of this study is to improve the $Tb-R$ distance scale by using a more precise, reliable, and larger calibration sample than that used by AIA15.

Stanghellini et al. (2020) proposed a PN statistical distance scale, based on the linear relationship between the nebular radius and H$_\beta$ surface brightness. This scale was calibrated using a PN sample of distances extracted from the Gaia DR2 parallaxes. This distance scale is defined as: $\log(R) = -(0.226 \pm 0.0155) \times \log(S_{Hb}) - (3.920 \pm 0.215)$, where R is the nebular radius in pc and S_{Hb} is the H$_\beta$ surface brightness.

Recently, Chornay & Walton (2021) released a catalog of 2118 CSs from Gaia EDR3. Examining the catalog, we found 424 and 351 PNe with unknown and negative parallaxes, respectively. From the remaining list, there are 67, 361, and 915 CSs of unknown, blue, and red colors, respectively.

The objectives of this article can be summarized as follows: (1) updating the $Tb-R$ distance scale presented in AIA15, applying a more accurate, homogenous, and reliable calibration sample of distances taken from Gaia EDR3; (2) comparing the PN Gaia parallaxes to past measurements in the literature; (3) examining the consistency between the trigonometric and other individual distance methods, based on larger statistical samples than presented in preceding studies. As a byproduct of this study, we detect the radial velocity (RV) of 14 PNe and the stellar variability of three PN CSs.

Sections 2 and 3 address the calibration sample as well as comparisons between Gaia and earlier parallax measurements. Section 4 discusses the consistency between the trigonometric and other individual distance methods, whereas Section 5 presents the new distance scale. Section 6 displays the identification of 14 CS RVs and stellar variability of three PN CSs, while the conclusion is given in Section 7.

2. The Calibration Sample

From ~3500 known Galactic PNe (Parker et al. 2012), there are 620 CSs that are spectroscopically confirmed as single/binary PN ionizing stars in the recent catalog of Weidmann et al. (2020). The catalog includes some misclassified objects such as EGB 4 (nova-like star), K 2–15 (H II region), WRAY 16–193 (symbiotic star), and LS III + 51 42 (emission-line star). The intense ultraviolet radiation output of most PN CSs causes them to appear as blue stars, however, there are many CSs that appear as red stars. This can be attributed to either the high reddening of its line of sight or the visible light being dominated by its close binary main sequence companion. Although the CS usually lies at the geometric center of the nebula, more evolved PNe and those interacting with the interstellar medium (ISM) have shown off-center shifts.

We restrict our search in the Gaia EDR3 database to the blue CSs of PNe that are listed in the HASH catalog (Parker et al.

2016) as true, possible, and likely PNe. In addition, we complement our sample with red CSs that have been spectro-scopically confirmed as PN nuclei by Weidmann et al. (2020). Further, we reject all matched Gaia sources of negative and missed parallax as well as those of unknown colors. We collect 603 matched Gaia sources. A part of this data set is given in Table 1, while the full table will be available online. Columns 1, 2, 3–4, and 5–6 provide the object name, Gaia EDR3 designation, equatorial coordinate, and Galactic coordinate, respectively. The parallax and proper motion and their uncertainties are given in columns 6–7 and 8–9, respectively. The stellar magnitudes G, B, R, and the B-R color index are listed in columns 10, 11, 12, and 13 respectively.

To obtain a high confidence calibrating sample, we select the true PNe from the HASH catalog with CSs of parallax errors less than 20%. The parallax measurements are corrected for the zero-point shift. Further, to recommend the goodness-of-fit indices for the Gaia EDR3 astrometry, we ignored the parallax measurements with a renormalized unit weight error (RUWE) larger than 1.4 (Fabricius et al. 2021). Finally, a total of 241 PNe are obtained. Unfortunately, only 95 PNe from this collection have published angular radius (θ) and 5 GHz radio surface flux (F_{5GHz}). This sample is used to re-calibrate the $Tb-R$ relationship. The farthest PN in the calibration sample is ~6000 pc away.

To test the new distance scale for calculating distances to remote nebulae, we support the calibration sample with the nebula "PS1", which belongs to the globular cluster "Pease 1". McNamara et al. (2004) calculated a distance of 9.98 kpc for this cluster, which is close to the traditional estimate of 10.4 kpc derived by Durrell & Harris (1993) but less than the distance of 11.2 kpc that was obtained by Kraft & Ivans (2003). In this study, we adopted the dynamical distance of 10.3 ± 0.4 kpc that was reported by van den Bosch et al. (2006) who developed orbit-based axisymmetric models for the globular cluster. These models matched 1264 line of sight velocity measurements (that extend out to 7′) and a sample of 703 proper motions (covering 0″25 of the inner cluster part). This enabled them to constrain the change in mass-to-light ratio as a function of radius and calculate the cluster's dynamical distance, inclination, central mass, and density of the cluster.

The full calibration sample will be available online, while a portion is presented in Table 2. The PNG number, PN common name, Gaia EDR3 designation, F_{5GHz} in mJy, θ in arcsecond, Gaia distance (D_G) in pc, PN radius (R) in pc, and Tb in K are given in columns 1, 2, 3, 4, 5, 6, 7, and 8, respectively. The predicated distance (D) in pc and its residual (see Section 5.1) are listed in columns 9 and 10, respectively.

In Figure 1, we compare the Gaia EDR3 distances with the calibrator distances adopted by AIA15 and FBP16 statistical scales. The comparison is based on 41 common objects between both calibration samples and Gaia EDR3. There is a clear match for numerous data points. Despite most of the

Table 1
Gaia EDR3 Sources that Matched True, Possible, and Likely PNe in the HASH Catalog

PN Name	Gaia Designation	l	b	α	δ	π_{Gaia}	μ_α	μ_δ	G mag	B mag	R mag	B-R
PN PC 12	Gaia EDR3 4 130 784 921 205 604 736	0.1660	17.2488	250.9741	−18.9533	0.052 ± 0.066	−3.17 ± 0.08	−2.37 ± 0.06	15.2	14.0	13.4	0.62
IC 4634	Gaia EDR3 4 126 115 570 219 432 448	0.3619	12.2147	255.3899	−21.8259	0.353 ± 0.043	−1.20 ± 0.05	−5.12 ± 0.03	13.9	12.3	12.4	−0.15
PN G000.7+08.0	Gaia EDR3 4 114 088 875 802 922 880	0.7176	8.0618	259.2877	−23.9416	0.045 ± 0.254	−3.39 ± 0.29	−5.42 ± 0.20	18.9	19.2	18.5	0.74
PN Bl 3–13	Gaia EDR3 4 056 540 677 880 158 208	0.9497	−2.0864	269.0116	−29.1880	0.150 ± 0.183	−1.96 ± 0.18	−5.51 ± 0.13	18.0	16.7	15.5	1.15
PN G001.2-05.6	Gaia EDR3 4 049 240 298 544 263 936	1.2146	−5.6614	272.7613	−30.7033	0.650 ± 0.422	−2.86 ± 0.44	−0.39 ± 0.35	18.6	18.5	18.2	0.35
PN H 1-47	Gaia EDR3 4 062 301 564 840 251 520	1.2949	−3.0402	270.1568	−29.3641	0.074 ± 0.052	1.32 ± 0.06	−7.02 ± 0.04	15.7	15.2	13.9	1.26
PN SwSt 1	Gaia EDR3 4 049 331 244 394 134 912	1.5906	−6.7176	274.0511	−30.8689	0.326 ± 0.110	−6.24 ± 0.13	−1.72 ± 0.09	11.8	11.0	10.1	0.85
PN H 1-55	Gaia EDR3 4 050 131 349 653 595 392	1.7136	−4.4554	271.8107	−29.6902	0.019 ± 0.860	−2.44 ± 0.78	1.41 ± 0.57	16.6	15.4	14.3	1.13
PN H 1-56	Gaia EDR3 4 050 126 711 087 206 016	1.7359	−4.6055	271.9745	−29.7429	0.075 ± 0.062	−4.00 ± 0.07	−9.42 ± 0.05	16.0	14.7	14.3	0.38
PN M 2-33	Gaia EDR3 4 049 596 604 655 713 664	2.0229	−6.2249	273.7773	−30.2593	0.224 ± 0.042	−0.06 ± 0.04	−6.03 ± 0.03	14.7	13.9	13.8	0.14

(This table is available in its entirety in machine-readable form.)

Table 2
The Calibration Sample

PNG	Name	Gaia designation	S5 GHz (mJy)	θ ($''$)	D_G (pc)	R (pc)	Tb (K)	D (pc)	$\|(D_G - D)/D_G\|\%$
PN G000.3+12.2	IC 4634	Gaia EDR3 4 126 115 570 219 432 448	114.8 ± 16.0	5.5 ± 1.10	2582 ± 288	0.069 ± 0.010	69.74 ± 17.00	3068 ± 182	18.8
PN G002.4+05.8	NGC 6369	Gaia EDR3 4 111 368 477 921 050 368	2002.0 ± 65.0	14.4 ± 2.88	1069 ± 56	0.075 ± 0.008	177.30 ± 35.92	912 ± 42	14.7
PN G002.7-52.4	IC 5148	Gaia EDR3 6 574 225 217 863 069 056	28.1 ± 3.5	62.5 ± 12.51	1145 ± 70	0.347 ± 0.041	0.13 ± 0.03	1443 ± 82	26.1
PN G009.4-05.0	NGC 6629	Gaia EDR3 4 089 517 157 442 187 008	266.0 ± 53.2	8.5 ± 1.69	1988 ± 90	0.082 ± 0.009	67.93 ± 15.19	2003 ± 106	0.7
PN G009.6+14.8	NGC 6309	Gaia EDR3 4 141 505 881 131 938 560	134.5 ± 26.9	8.8 ± 1.75	2500 ± 401	0.106 ± 0.020	31.98 ± 7.15	2364 ± 125	5.4
PN G011.3-09.4	PN H 2-48	Gaia EDR3 4 078 224 382 749 921 024	66.8 ± 7.0	2.3 ± 0.11	4365 ± 738	0.049 ± 0.009	231.20 ± 32.79	5312 ± 191	21.7
PN G011.7-00.6	NGC 6567	Gaia EDR3 4 094 749 870 714 268 544	159.6 ± 12.5	3.8 ± 0.01	2725 ± 260	0.050 ± 0.005	202.84 ± 15.89	3334 ± 71	22.4
PN G016.4-01.9	PN M 1-46	Gaia EDR3 4 103 910 524 954 236 928	83.5 ± 9.0	5.8 ± 1.16	2303 ± 84	0.064 ± 0.007	45.82 ± 10.41	3262 ± 176	41.6
PN G017.6-10.2	PN A66 51	Gaia EDR3 4 086 643 583 803 222 400	29.0 ± 5.8	31.6 ± 6.31	1758 ± 95	0.269 ± 0.031	0.53 ± 0.12	1966 ± 104	11.8
PN G025.3+40.8	IC 4593	Gaia EDR3 4 457 218 245 479 455 744	92.0 ± 18.0	7.0 ± 1.39	2546 ± 294	0.086 ± 0.013	34.86 ± 9.75	2916 ± 204	14.5

(This table is available in its entirety in machine-readable form.)
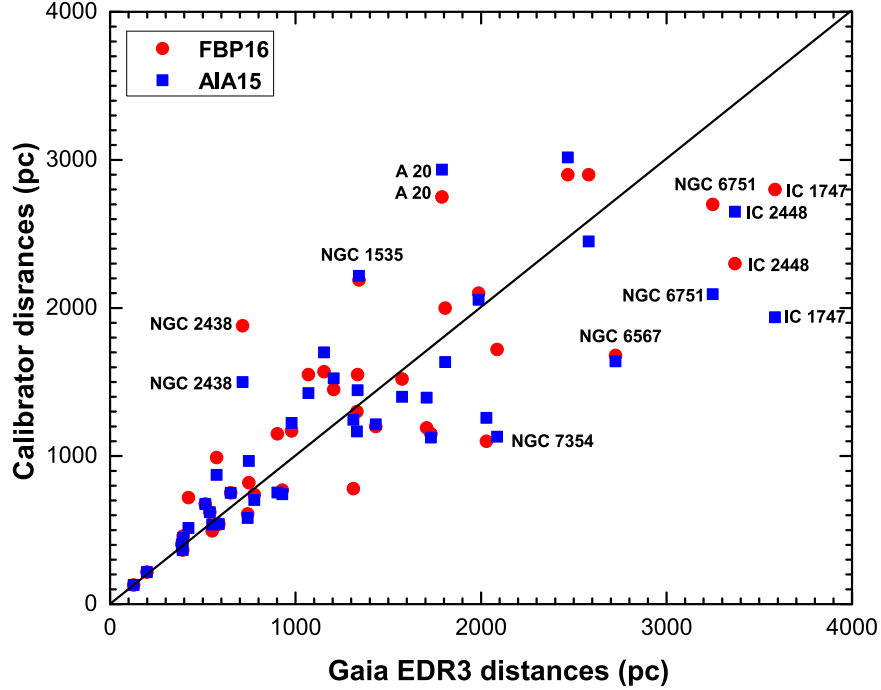
Figure 1. The Gaia EDR3 vs. AIA15 and FBP16 calibration samples.

objects being clustered around the 1:1 line, there are a few exceptions, including IC 1747, NGC 2438, NGC 2438 and A 20. We estimate the median distance ratio between both calibrator samples and Gaia EDR3, where the results reveal that AIA15 and FBP16 distance scales slightly underestimate (0.98) and overestimate (1.06) the PN Gaia distance, respectively. This comparison is limited to PNe with distance less than ∼3600 pc.

3. Gaia Versus Prior Parallax Measurements

Surveying the literature, there were ∼40 ground and space-based trigonometric PN parallaxes known prior to the Gaia period. Acker et al. (1998) provided the Hipparcos parallax (π_{HIP}) measurements for a set of 19 PNe, two of which had questionable parallaxes (SwSt 1 & Hu 2–1). In general, the parallax accuracy of this set of CSs is relatively poor since their magnitudes are close to the magnitude limit of the Hipparcos observatory. Another set of 16 PN parallaxes (π_{USNO}) has been measured through the US Naval Observatory (USNO) parallax program (Harris et al. 2007). Twelve objects in this set had parallax errors less than 20%. Using the Hubble Space Telescope (HST), Benedict et al. (2009) reported highly accurate parallaxes (π_{HST}) of four PNe. We derive median parallax errors of 2.5 mas, 0.42 mas, and 0.23 mas for the Hipparcos, USNO, and HST PN sets, respectively. The Gaia parallaxes are compared to the HST and USNO parallaxes in Figure 2. In both graphs, the solid diagonal line indicates the

1:1 matches, while the dashed line illustrates the linear fitting which demonstrates a tight correlation between both the HST and USNO and the Gaia parallaxes. The HST parallaxes appear marginally smaller than the Gaia ones (Figure 2, left panel), whereas a few USNO parallaxes are larger and others are slightly smaller than the Gaia parallaxes (Figure 2, right panel). The median scaling factors $\langle \pi_{\mathrm{HST}}/\pi_{\mathrm{Gaia}} \rangle$ and $\langle \pi_{\mathrm{USNO}}/\pi_{\mathrm{Gaia}} \rangle$ are 0.9 and 1.0, respectively. The median errors of the HST and USNO parallaxes are ∼4.0 and ∼8.0 times that of Gaia (0.053 mas), respectively. In contrast to the HST and USNO results, the Hipparcos shows a small median scaling factor $\langle \pi_{\mathrm{HIP}}/\pi_{\mathrm{Gaia}} \rangle$ of 0.6. Furthermore, the median error of Hipparcos is ∼40 times that of Gaia. In this analysis, we adopt only π_{Gaia} measurements with uncertainties less than 15%.

4. Gaia Distances Versus Other Individual Distances

As previously stated, a limited number of PN parallaxes were known prior to the Gaia mission. As a result, the previous studies on the topic of consistency between trigonometric and other individual distance methods are statistically unreliable. In AIA15, we compared directly the PN trigonometric distances to the extinction and gravity distances and indirectly, due to the small number of common objects, to the spectroscopic, expansion, photoionization, and kinematic distances. The currently available number of PNe parallaxes is suitable to conduct such a study based on a statistically better basis. Moreover, to make such analyses more reliable than past ones,
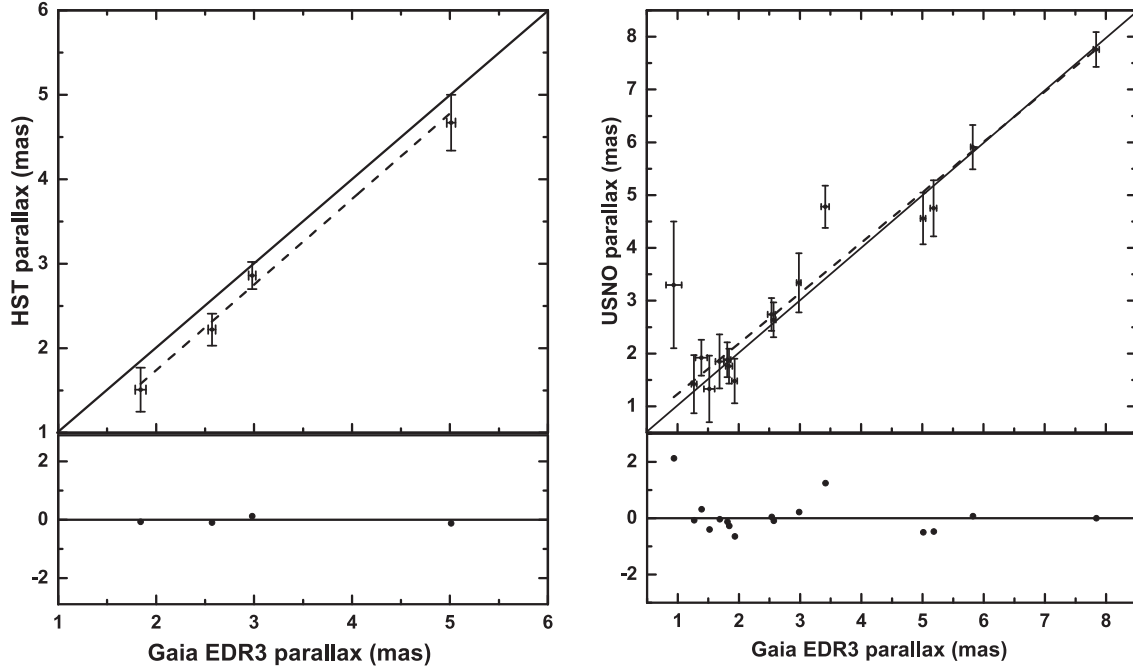
Figure 2. The Gaia EDR3 against HST (left panel) and USNO (right panel) parallaxes. The solid and dashed lines indicate the 1:1 matches and linear fitting, respectively. The fitting residual is given below each graph.

Table 3
The Mean and Median Scaling Ratios, Correlation Coefficient (r), and the Probability p-value between the Individual Methods and the Trigonometric Method

Method	Spectroscopic	Expansion	Extinction	Gravity	Photoionization	Kinematic
# Objects	23	19	27	53	20	19
Mean	1.10	1.00	0.92	1.14	1.24	0.88
Median	1.10	0.99	0.75	1.06	1.10	0.91
r	0.78	0.83	0.46	0.84	0.53	0.74
p-value	1.02E-05	1.35E-05	1.45E-02	0.00E+00	1.71E-02	3.01E-04

we adopt only Gaia distances with uncertainties less than 25%. We found 23, 19, 27, 53, 20, and 19 common objects between the trigonometric and spectroscopic, expansion, extinction, gravity, photoionization, and kinematic methods, respectively.

Figure 3 (top left panel) displays the spectroscopic against trigonometric distances. The comparison shows that there is a discrepancy between the two techniques for determining the distances for about half the common sample. The spectroscopic approach overestimates the distances of a few objects, e.g., Me 1-1, while underestimating the distances of others, e.g., K 1-27 and A79. The median scaling ratio ⟨*spectroscopic/trigono-metric*⟩ indicates that the spectroscopic technique marginally overestimates the trigonometric distances.

The comparison between the expansion and trigonometric distances is present in Figure 3 (top right panel). Except for a few objects (e.g., IC 2448, NGC 5979, and NGC 6891), the distances of most PNe are marginally consistent. The derived median scaling ratio ⟨*expansion/trigonometric*⟩ is 0.99. The

linear regression exhibits a strong correlation between both distance methods (see Table 3).

In Figure 3 (middle left panel), we compare the extinction with trigonometric distances. The inconsistency between the two methods is obvious. The extinction method underestimates the distances of more than half the common objects. The median distance ratio is 0.75. This result differs from that mentioned in AIA15, which shows a median ratio of 1.0. In support of this result, Dharmawardena et al. (2021) derived the extinction distances for a collection of 17 PNe by applying three distinct 3D extinction mapping methods and comparing them to the Gaia DR2. We estimate the median distance ratios for the proposed three methods, which are 0.63, 1.1, and 0.83 with an average of 0.85.

Our analysis here is based on a larger statistical sample than that given by AIA15 and Dharmawardena et al. (2021). Because the usage of this method is limited to objects near the Galactic plane, we exclude objects at high Galactic latitudes
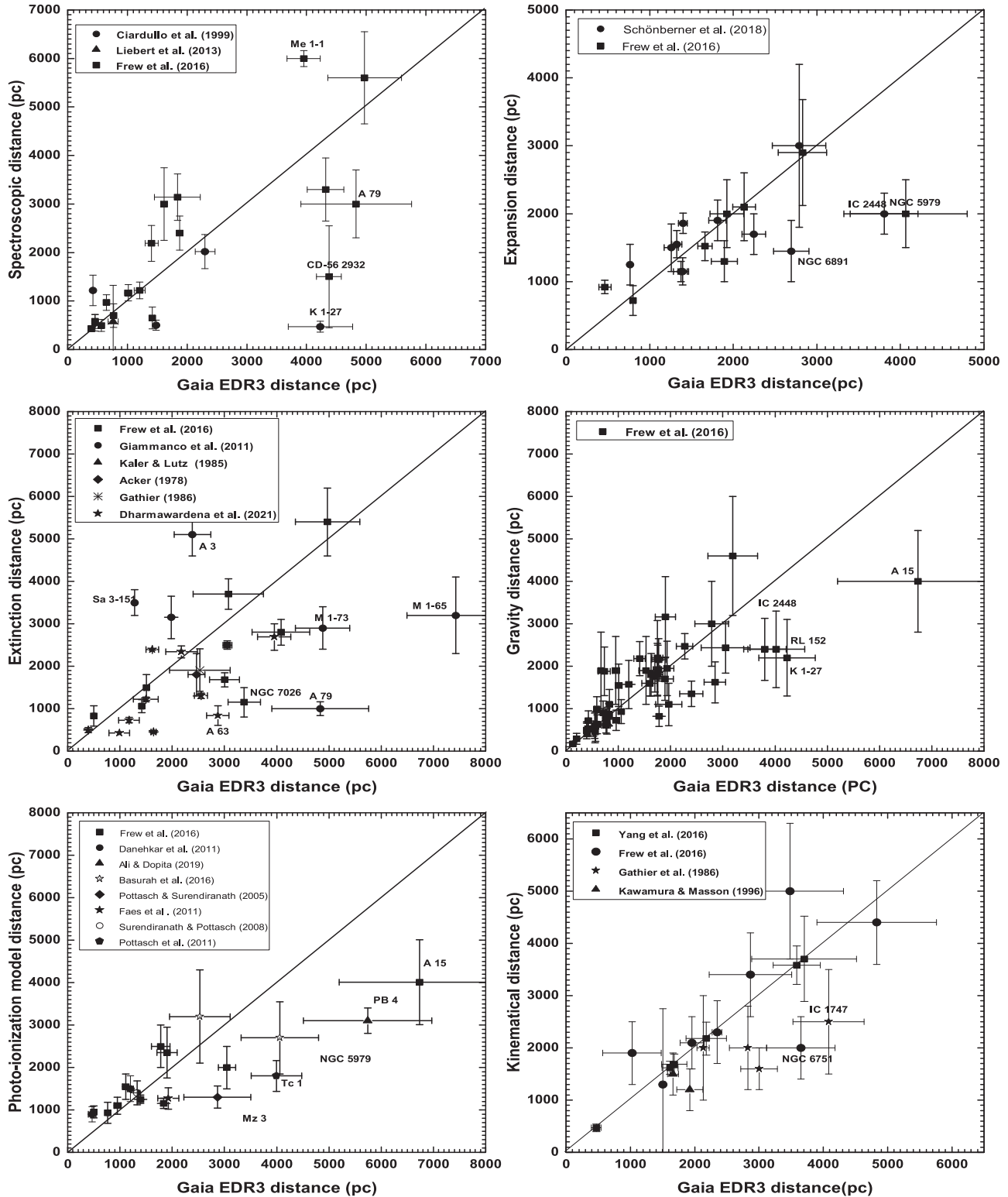
Figure 3. Comparisons between the trigonometric and other individual distance methods. The Gaia vs. spectroscopic distance is illustrated in the upper left panel, expansion distance in the upper right panel, extinction distance in the middle left panel, gravity distance in the middle right panel, photoionization model distance in the lower left panel, and kinematical distance in the lower right panel. In each graph, we distinguished only the names of outlier objects. The references for the individual distances are as follows: Ciardullo et al. (1999); Liebert et al. (2013); FBP16; Schönberner et al. (2018); Giammanco et al. (2011); Kaler & Lutz (1985); Acker (1978); Gathier et al. (1986b); Dharmawardena et al. (2021); Danehkar et al. (2012); Ali & Dopita (2019); Basurah et al. (2016); Pottasch & Surendiranath (2005); Faes et al. (2011); Surendiranath & Pottasch (2008); Pottasch et al. (2011);Yang et al. (2016); FBP16; Gathier et al. (1986a); Kawamura & Masson (1996).
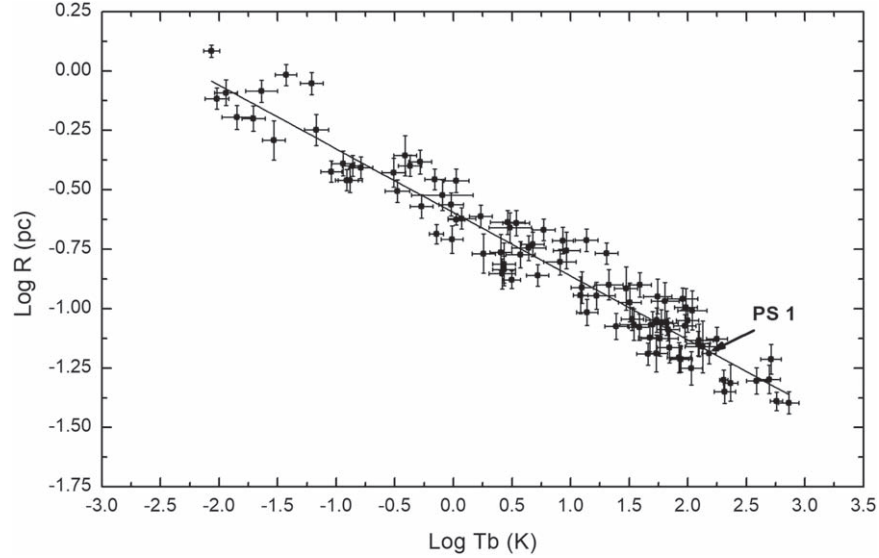
Figure 4. The *Tb-R* relationship, based on the Gaia EDR3 calibrating sample. The black arrow shows the location of the "PS 1" nebula on the *Tb-R* relationship.

from our analysis, to avoid underestimating their distances. The linear fitting also reveals a weak correlation between the two methods ($r = 0.38$). Therefore, caution should be taken when applying this method to determine the PN distances.

The comparison between the gravity and trigonometric methods is plotted in Figure 3 (middle right panel). The plot indicates the majority of objects have inconsistent distances, e.g., A15, K 1–27, RL 152, and IC 2448. In comparison to the trigonometric technique, the result reveals a slight overestimate of the gravity method, whereas the median distance ratio is 1.06. This result differs from the prior values of 0.65, 0.60, 0.77, and 0.81 provided by Napiwotzki (2001), Jacoby & van de Steene (1995), Harris et al. (2007), and AIA15, respectively. Smith (2015) suggested that the gravity method is distance-dependent, meaning that it overestimates the distance to nearby objects while underestimating the distance to remote objects. Figure 3 (middle right panel) confirms this result, where the gravity method gives overestimation and underestimation for the PNe of distances less than and greater than 3000 pc, respectively. It is significant to note here that all gravity distances used in this comparison are compiled from FBP16, where they established an internally consistent data set using appropriate and modified parameters better than prior ones found in the literature.

The photoionization distances are compared with the trigonometric distances in Figure 3 (lower left panel). The figure demonstrates the photoionization method underestimates the distances of objects at a distance roughly less than 2000 pc while overestimating the distances of objects farther than 2000 pc. In general, there is a clear inconsistency between the distances determined by both methods.

The distances computed by the kinematical method are compared to those derived by the trigonometric method in Figure 3 (lower right panel). The figure shows that the consistency between both methods is higher than the other methods discussed above. The mean scaling ratio and the correlation coefficient between both methods indicate a good match.

Summarizing the previous results, there is inconsistency between the trigonometric and the spectroscopic, extinction, gravity, and photoionization model distance methods. The expansion and kinematical methods show moderate consistency with the trigonometric method. Table 3 compares the mean and median scaling ratios, correlation coefficients (r), and probability p-values (for a null correlation) of the individual methods to the trigonometric method. The evaluated p-values for all individual methods provide strong evidence against null correlations.

5. The New Distance Scale

5.1. Tb−R Relationship

The $Tb−R$ relationship was first applied by van de Steene & Zijlstra (1995) and then used by others as a tool for measuring the PN statistical distance. Here, we reconstruct this relationship, where the estimation of the Tb and R parameters is based on a precise Gaia distance sample. The Tb and R are estimated using equations 2 and 6 in AIA15. Figure 4 shows a tight anti-correlation ($r = -0.97$) between both parameters. The solid line represents the linear regression of the data points. The position of the distant nebula PS1 is indicated by a black arrow in the lower right side of Figure 4. It is evident that the linear fitting does not rely on this distant nebula. From the linear
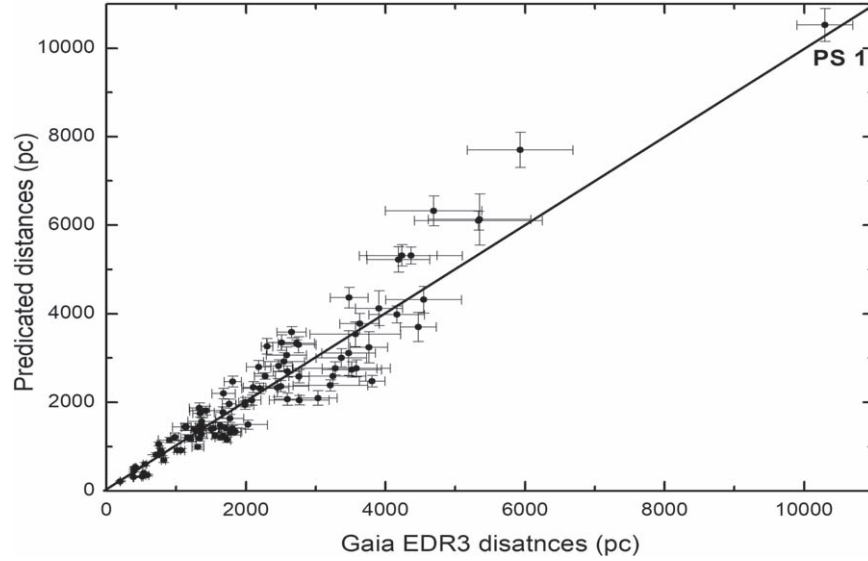
Figure 5. Predicted vs. calibrated distances. The solid line indicates the 1:1 matches.

fitting, we derive the equation of the new distance scale: it is evident that the linear fitting does not rely on this distant nebula.

$$\log(D) = 1.3817 - 0.465 \log \theta - 0.268 \log F_{5\text{GHz}}.$$

Here θ, $F_{5\text{GHz}}$, and D are as previously defined. The uncertainty of Tb and R is calculated by propagating the error in the angular radius, radio flux and PN distance. To measure the quality of this approach, we compare the calibration distance (D_{Gaia}) with the predicted distance (D) in Figure 5. The predicted distance of the distant "PS1" nebula according to the new scale is $10\,521 \pm 373$, which is 2.1% more than the nebula's adopted distance. In general, the new distance scale slightly overestimates the PN with distances of 4.5–6.0 kpc. Therefore, we should take caution about the distances of objects larger than 4500 pc. The mean and median absolute distance residuals (($D_G - D$)/D_G) are respectively 18.0% and 17.0%. This result implies that the mean error in the predicted distances is $\sim$18.0%, indicating that the accuracy of the new scale is better than the prior distance scales. The dispersion of the distance scale reported by Stanghellini et al. (2008), e.g., is greater than 30%. AIA15 obtained an accuracy of 28.7% for the Tb-R distance scale, while FBP16 determined distance dispersions of 28% and 18% for optically thick and thin PNe, respectively, with a mean accuracy of 23% for the entire distance scale.

5.2. Distance Catalog

In Table 4, we present a portion of the Galactic PN statistical distance catalog which contains $\sim$1000 PNe. The entire catalog will be available online. Columns 1, 2–3, and 4–5 give the PN common name, equatorial coordinates, and Galactic coordinates, respectively. Columns 6 and 7, respectively, list the

adopted $F_{5\text{GHz}}$ and θ measurements and their associated errors. The predicted distances and their associated errors are stated in columns 8, while in columns 9, 10, and 11 we present the distances derived by AIA15, FBP16, and Stanghellini et al. (2020), for comparison. This catalog will be a significant source for future PN investigations and a useful guide for the PNe of unknown and unreliable distances.

Examining the prior PN distance scales reveals they are graded as long or short depending on whether they overestimate or underestimate the PN distances. Following Phillips (2002), we calculate the correlation coefficient and the relative scale ratio factor (κ) between the present distance scale and some commonly used distance scales. The result is displayed in Table 5. In general, the present distance scale is compatible with others within the error range. Nonetheless, it is longer than Cahn et al. (1992), van de Steene & Zijlstra (1995), AIA15, and Stanghellini et al. (2020), but shorter than Zhang (1995) and FBP16. The results of AIA15 and FBP16 presented in Table 5 reflect the previous results raised in Section 2 regarding the calibrator sample of both scales.

6. Central Stars' Radial Velocity and Variability

The stellar RV and variability that are given in Gaia EDR3 were referenced from Gaia DR2. The upcoming full third release of the Gaia mission is expected to witness new measurements for both parameters as well as updating existing estimations. In general, the RV of PNe is measured by the Doppler shift of their emission spectral lines (Durand et al. 1998). Accurate measurement requires a high-dispersion nebular spectrum. Gaia offers yet another mechanism for measuring the RV using the Doppler shift of the central star

Table 4
Distance Catalog

| PN Name | Galactic Coordinate | | Equatorial Coordinate | | F_{5GHz} (mJy) | Angular Radius (arcseconds) | Distance (pc) | | | |
	L	B	α	δ			This work	Ali et al. (2015)	Frew et al. (2016)	Stanghellini et al. (2020)
PN M 1–51	20.9993	−1.1251	278.371	−11.124	319.0 ± 32.0	6.7 ± 1.3	2125 ± 206	1847 ± 175	2310 ± 750	2270 ± 740
IRAS 18 252-1016	21.1653	0.4755	277.006	−10.236	131.7 ± 12.4	1.2 ± 0.0	6042 ± 153	4721 ± 176		
PN M 1-63	21.1704	−5.9834	282.879	−13.177	10.0 ± 2.0	2.1 ± 0.4	9294 ± 997	8452 ± 914		
IRAS 18 303-1043	21.3425	−0.8423	278.277	−10.689	17.6 ± 2.7	1.3 ± 0.2	10079 ± 791	8595 ± 732		
VSP 2-19	21.6657	0.8109	276.940	−9.637	52.9 ± 4.8	0.7 ± 0.1	9641 ± 411	7519 ± 387		
IRAS 18 305-1022	21.6850	−0.7376	278.343	−10.337	36.5 ± 6.0	3.8 ± 0.0	4921 ± 218	4466 ± 250		
PN M 3-55	21.7431	−0.6726	278.312	−10.255	19.0 ± 3.8	8.8 ± 1.8	3984 ± 427	3976 ± 392	5860 ± 2460	6270 ± 2630
PN M 3–28	21.8201	−0.4778	278.172	−10.097	33.4 ± 3.9	4.7 ± 0.2	4571 ± 162	4236 ± 176	3610 ± 1140	3860 ± 1220
IRAS 18 316-1010	21.9972	−0.8837	278.621	−10.127	14.2 ± 1.7	1.2 ± 0.1	10694 ± 557	9198 ± 535		
PN M 1-58	22.0710	−3.1853	280.737	−11.115	60.0 ± 25.0	3.2 ± 0.6	4687 ± 680	4106 ± 701		

(This table is available in its entirety in machine-readable form.)

Table 5
Scaling Factors for Seven Different Distance Scales in the Literature

Statistical scale	κ	r	N
Cahn et al. (1992)	0.79 ± 0.23	0.73	1008
van de Steene & Zijlstra (1995)	0.94 ± 0.24	0.94	1008
Zhang (1995)	1.02 ± 0.32	0.91	1008
Stanghellini et al. (2008)	1.04 ± 0.22	0.95	1008
Ali et al. (2015)	0.95 ± 0.11	0.99	1008
Frew et al. (2016)	1.02 ± 0.38	0.88	612
Stanghellini et al. (2020)	0.93 ± 0.34	0.81	229

Table 6
PNe RVs from Gaia EDR3

Object Name	Gaia EDR3 Designation	RV (km s^{-1})	
		Gaia EDR3	Durand et al. (1998)
A 35	3499149202247569536	-40.5 ± 5.8	-6.6 ± 3.8
H 3-75	3340384082588168960	6.9 ± 9.0	22.9 ± 2
K 1-14	4556040392088375168	-19.1 ± 2.4	
K 1-6	2288467186442571008	-47.4 ± 10.7	
K 2-7	6868431267915481088	-17.8 ± 0.4	
LoTr 1	2917223705359238016	19.3 ± 3.2	
LoTr 5	3958428334589607552	-10.5 ± 1.6	
M 1-2	360112911622101120	-22.9 ± 19.6	-12.1 ± 2
M 1-44	4052553745525657600	-4.3 ± 1.1	-107.7 ± 23.4
Pe 1-11	4042468784326846336	-12.0 ± 0.3	-130.6 ± 14
PHR J0701-0749	3052395775097859072	46.3 ± 4.1	
PN G019.5-04.9	4105051680543027584	-23.6 ± 0.7	
SaSt 2-12	5923760667266961408	-67.0 ± 1.6	-63 ± 0.5
WeBo 1	465640807845756160	-11.6 ± 16.2	

spectral lines. As a byproduct of extracting the PN parallaxes, we detect the RV for 14 CSs. Table 6 compares this result with the available nebular RVs in Durand et al. (1998). The stellar RV of SaSt 2–12 is the only one that is consistent with the RV of its host nebula, whereas the other five objects exhibit discrepancies. Moreover, we detect the CS variability of ETHOS 1, HFG1, and Hen 2–447. ETHOS 1 is a close binary CS with an orbital period of 0.535 d and an extremely large amplitude (Miszalski et al. 2011). HFG1 is a close detached pre-cataclysmic binary in which the CS binary components consist of a primary O-type subdwarf and a secondary F5-K0 main sequence star (Chiotellis et al. 2016). To our knowledge, the variability of the Hen 2–447 central star has been detected for the first time.

7. Conclusions

We established a new distance scale for PNe by re-calibrating the $Tb-R$ relationship with 96 CSs, the distances of which were estimated using Gaia EDR3 trigonometric parallaxes. The advantage of using this calibration sample is

that all distances are obtained utilizing a single approach. Moreover, all the calibrators have uncertainties in their distances less than 20%. As a result, we created a statistical distance catalog for ~1000 PNe. In addition, we investigated the consistency between the trigonometric and other individual distance methods, whereas we found that most of the PN distances obtained by these methods are incompatible with the trigonometric method. The expansion and kinematical distance methods showed better consistency than other methods. In contrast to previous results in the literature, we found the extinction method underestimates the PN distances by ~25% on average. This result is relatively consistent with the recent results of Dharmawardena et al. (2021). The gravity method showed overall comparable distances to the trigonometric method but differed from the previous findings in the literature that indicated that this method underestimates the PN distances. As a byproduct of extracting the PN parallaxes from the Gaia EDR3 database, we identified the RV for 14 PN CSs and the variability for three PN CSs, one of which was found for the first time.

ORCID iDs

A. Ali ⓘ https://orcid.org/0000-0003-4180-8420

References

Acker, A. 1978, A&AS, 33, 367
Acker, A., Fresneau, A., Pottasch, S. R., & Jasniewicz, G. 1998, A&A, 337, 253
Ali, A., & Dopita, M. A. 2019, MNRAS, 484, 3251
Ali, A., Ismail, H. A., & Alsolami, Z. 2015, Ap&SS, 357, 21
Basurah, H. M., Ali, A., Dopita, M. A., et al. 2016, MNRAS, 458, 2694
Benedict, G. F., McArthur, B. E., Napiwotzki, R., et al. 2009, AJ, 138, 1969
Brown, A. G. A., et al. 2021, A&A, 650, 7
Cahn, J. H., Kaler, J. B., & Stanghellini, L. 1992, A&AS, 94, 399
Chiotellis, A., Boumis, P., Nanouris, N., Meaburn, J., & Dimitriadis, G. 2016, MNRAS, 457, 9
Chornay, N., & Walton, N. A. 2021, A&A, 656, A110
Ciardullo, R., Bond, H. E., Sipior, M. S., et al. 1999, AJ, 118, 488
Danehkar, A., Frew, D. J., Parker, Q. A., & De Marco, O. 2012, IAUS, 283, 340
Dharmawardena, T. E., Barlow, M. J., Drew, J. E., et al. 2021, MNRAS, 501, 6156
Durand, S., Acker, A., & Zijlstra, A. 1998, A&AS, 132, 13
Durrell, P. R., & Harris, W. E. 1993, AJ, 105, 1420
Fabricius, C., Luri, X., Arenou, F., et al. 2021, A&A, 649, A5
Faes, D. M., Costa, R. D. D., & Morisset, C. 2011, Revista Mexicana de Astronomia y Astrofisica Conference Series, 40, 233
Frew, D. J., Parker, Q. A., & Bojičić, I. S. 2016, MNRAS, 455, 1459
Gathier, R., Pottasch, S. R., & Goss, W. M. 1986a, A&A, 157, 191

Gathier, R., Pottasch, S. R., & Pel, J. W. 1986b, A&A, 157, 171
Giammanco, C., Sale, S. E., Corradi, R. L. M., et al. 2011, A&A, 525, A58
Harris, H. C., Dahn, C. C., Canzian, B., et al. 2007, AJ, 133, 631
Jacoby, G. H., & van de Steene, G. 1995, AJ, 110, 1285
Kaler, J. B., & Lutz, J. H. 1985, PASP, 97, 700
Kawamura, J., & Masson, C. 1996, ApJ, 461, 282
Kraft, R. P., & Ivans, I. I. 2003, PASP, 115, 143
Liebert, J., Bond, H. E., Dufour, P., et al. 2013, ApJ, 769, 32
Lindegren, L., Hernández, J., Bombrun, A., et al. 2018, A&A, 616, A2
Lindegren, L., Bastian, U., Biermann, M., et al. 2021, A&A, 649, A4
McNamara, B. J., Harrison, T. E., & Baumgardt, H. 2004, ApJ, 602, 264
Miszalski, B., Corradi, R. L. M., Boffin, H. M. J., et al. 2011, MNRAS, 413, 1264
Napiwotzki, R. 2001, A&A, 367, 973
Parker, Q. A., Bojičić, I. S., & Frew, D. J. 2016, Journal of Physics Conference Series, 728, 032008
Parker, Q. A., Frew, D. J., Acker, A., & Miszalski, B. 2012, IAUS, 283, 9

Phillips, J. P. 2002, ApJS, 139, 199
Pottasch, S. R., & Surendiranath, R. 2005, A&A, 444, 861
Pottasch, S. R., Surendiranath, R., & Bernard-Salas, J. 2011, A&A, 531, A23
Schönberner, D., Balick, B., & Jacob, R. 2018, A&A, 609, A126
Smith, H. 2015, MNRAS, 449, 2980
Stanghellini, L., Bucciarelli, B., Lattanzi, M. G., & Morbidelli, R. 2020, ApJ, 889, 21
Stanghellini, L., Shaw, R. A., & Villaver, E. 2008, ApJ, 689, 194
Surendiranath, R., & Pottasch, S. R. 2008, A&A, 483, 519
van de Steene, G. C., & Zijlstra, A. A. 1995, A&A, 293, 541
van den Bosch, R., de Zeeuw, T., Gebhardt, K., Noyola, E., & van de Ven, G. 2006, ApJ, 641, 852
Weidmann, W. A., Mari, M. B., Schmidt, E. O., et al. 2020, A&A, 640, A10
Yang, A. Y., Tian, W. W., Zhu, H., Leahy, D. A., & Wu, D. 2016, ApJS, 223, 6
Zhang, C. Y. 1995, ApJS, 98, 659